AD-A137 981 AN ANALYSIS OF THE COAX-FED MONOPOLE IN A GENERAL MEDIUM(U) MISSISSIPPI UNIV UNIVERSITY DEPT OF ELECTRICAL ENGINEERING C M BUTLER ET AL. 25 DEC 83 1/1

UNCLASSIFIED NOSC-CR-220 N66001-82-C-0045 F/G 9/1 NL

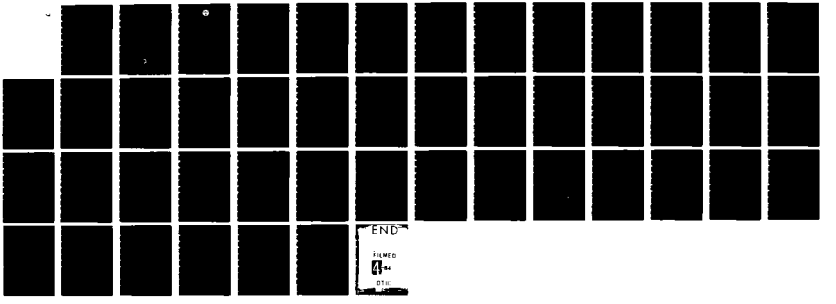

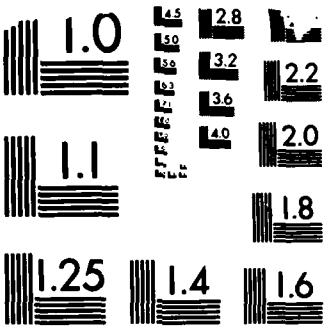

MICROCOPY RESOLUTION TEST CHART
NATIONAL BUREAU OF STANDARDS-1963-A

NOSC CR 220

AD A137981

Contractor Report 220

AN ANALYSIS OF THE COAX-FED MONOPOLE IN A GENERAL MEDIUM

C. M. Butler
K. A. Michalski
S. Filipovic

December 1983
Final Report
March 1982 — June 1983

Prepared for
Naval Ocean Systems Center
Code 811

Sponsored by
Naval Electronic Systems Command
PME 117

NOSC
NAVAL OCEAN SYSTEMS CENTE
San Diego, California 921

NAVAL OCEAN SYSTEMS CENTER SAN DIEGO, CA 92152

AN ACTIVITY OF THE NAVAL MATERIAL COMMAND

J.M. PATTON, CAPT, USN
Commander

R.M. HILLYER
Technical Director

ADMINISTRATIVE INFORMATION

Administrative information pertaining to Naval Ocean Systems Center Contractor Report 220 is listed below.

Item	Data
Performing Organization	Department of Electrical Engineering University of Mississippi University, MS 38677
Contract Number	N66001-82-C-0045
Controlling Office	Naval Ocean Systems Center Code 8112 San Diego, CA 92152
Sponsor	Naval Electronic Systems Command(PME 117), Washington, DC 20360 in conjunction with U.S. Army Headquarters Communications Electronic Engineering Installation Agency, 1900 Half St. SW, Washington, DC 20324
Program Element	OMN

The contracting officers' technical representative was James C. Logan, NOSC Code 8112.

Released by
M. S. Kvigne, Head
Communications and Technology Division

Under authority of
H. F. Wong, Head
Communications Systems and Technology Department

TJ

UNCLASSIFIED

SECURITY CLASSIFICATION OF THIS PAGE (When Data Entered)

REPORT DOCUMENTATION PAGE	READ INSTRUCTIONS BEFORE COMPLETING FORM
1. REPORT NUMBER: NOSC CR 220	2. GOVT ACCESSION NO.: AD-A137981
	3. RECIPIENT'S CATALOG NUMBER:
4. TITLE (and Subtitle): AN ANALYSIS OF THE COAX-FED MONOPOLE IN A GENERAL MEDIUM	5. TYPE OF REPORT & PERIOD COVERED: Final, March 15, 1982—June 20, 1983
	6. PERFORMING ORG. REPORT NUMBER:
7. AUTHOR(s): C.M. Butler, K.A. Michalski, S. Filipovic	8. CONTRACT OR GRANT NUMBER(s): N66001-82-C-0045
9. PERFORMING ORGANIZATION NAME AND ADDRESS: Department of Electrical Engineering, University of Mississippi, University, MS 38677	10. PROGRAM ELEMENT, PROJECT, TASK AREA & WORK UNIT NUMBERS: OMN
11. CONTROLLING OFFICE NAME AND ADDRESS: Naval Ocean Systems Center, San Diego, CA 92152	12. REPORT DATE: July 25, 1983
	13. NUMBER OF PAGES: 42
14. MONITORING AGENCY NAME & ADDRESS (if different from Controlling Office): Naval Electronic Systems Command (PME117), Washington, D.C. 20360 with US Army Headquarters Communications Electronic Eng. Installation Agency, Washington, DC 20324	15. SECURITY CLASS. (of this report): Unclassified
	15a. DECLASSIFICATION/DOWNGRADING SCHEDULE:

16. DISTRIBUTION STATEMENT (of this Report)

Approved for public release; distribution unlimited

17. DISTRIBUTION STATEMENT (of the abstract entered in Block 20, if different from Report)

18. SUPPLEMENTARY NOTES

19. KEY WORDS (Continue on reverse side if necessary and identify by block number)

Electromagnetic fields and waves
Monopole antenna
Antenna in lossy medium

20. ABSTRACT (Continue on reverse side if necessary and identify by block number)

A coax-fed monopole antenna in a general linear medium is investigated theoretically and results are corroborated experimentally. The monopole resides in a general lossy medium above a ground plane and is formed by the extension of the center conductor of a coaxial waveguide whose outer conductor terminates in the ground plane. The excitation is the usual TEM field in a coax. The analysis is sufficiently general to accommodate a bead of prescribed dielectric properties to support and center the coax inner conductor. Coupled integral equations are derived for the monopole current and for the electric field in the annular aperture formed where the coaxial guide joins the ground plane. These equations account for the higher order modes in the .

(Continued on reverse side)

DD FORM 1 JAN 73 1473 EDITION OF 1 NOV 65 IS OBSOLETE

S/N 0102-LF-014-6601

UNCLASSIFIED

SECURITY CLASSIFICATION OF THIS PAGE (When Data Entered)

20. Continued
coaxial guide. A numerical/analytical method for solving these coupled equations is developed and implemented. Numerical results—monopole current, aperture electric field, and driving point admittance—are obtained and are compared with available experimental data. The agreement is generally excellent.

TABLE OF CONTENTS

LIST OF FIGURES

1. INTRODUCTION

In this report, a coax-fed monopole antenna completely immersed in water is investigated theoretically and the results are corroborated experimentally. The major thrust of the investigation is to acquire a better understanding of the properties of the current on an antenna in a lossy medium. Coupled integral equations are derived for the current on the antenna and the electric field in the aperture formed where the coaxial guide joins the conducting ground plane (Fig. 1). These equations accurately characterized the above-mentioned current and electric field for the structure illustrated in the figure. Numerical/analytical techniques needed to solve thse equations are developed in the report. Numerical results are obtained and are compared with experimental data available elsewhere. These equations and the numerical techniques developed for solving them provide the basis upon which one may found an accurate analysis of an antenna in a lossy medium.

The monopole antenna illustrated in Fig. 1 is the extension of the center conductor of a coaxial waveguide whose outer conductor terminates at the conducting ground plane. The monopole is taken to be a conducting tube (open-ended) with a vanishingly thin wall. It is fed or driven by a time-harmonic signal ($e^{j\omega t}$) from the coaxial guide and receives its excitation through the annular aperture where the coax opens into the ground plane. The monopole is of height h and radius a and it resides in a semi-infinite, homogeneous medium characterized by (μ,ε) with ε $(= \varepsilon_0\varepsilon_r - j\frac{\sigma}{\omega})$ allowed to be complex to account for losses. The

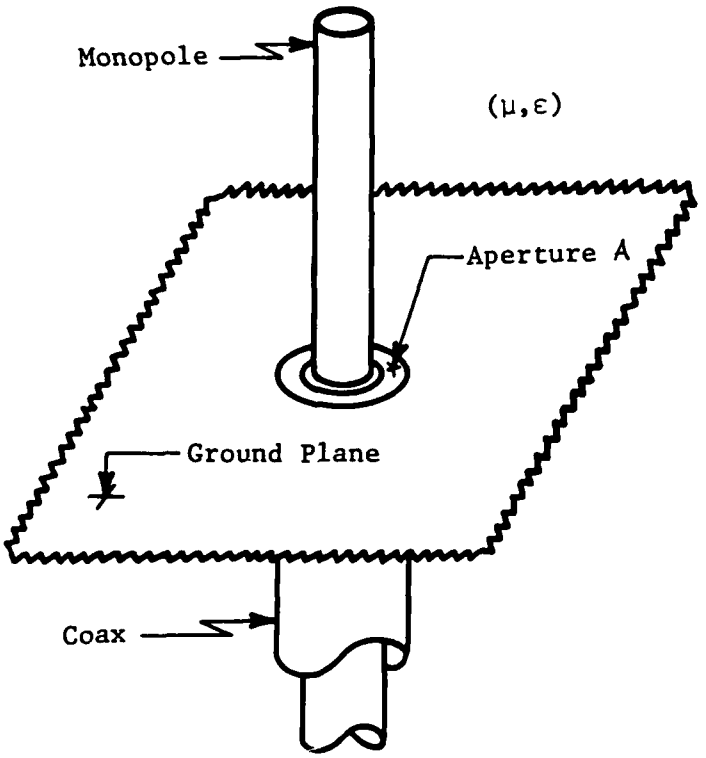

Fig. 1. Coax-fed monopole above a ground plane.

radii of the inner and outer coax conductors are a and b, respectively, and the medium in the annular region between the conductors may be uniform in which case it is characterized by (μ_c,ε_c) or it may be a gas (μ_g,ε_g) in which a dielectric (μ_c,ε_c) bead of length L is inserted to provide mechanical support. (See Fig. 2 .) In the former case of a uniform solid dielectric, L is made to approach infinity. As suggested in Fig. 2 , the monopole radius may differ from that of the coax inner conductor.

We wish to calculate the current induced in the monopole and to determine the load, or admittance, which the monopole presents to the coaxial line. The known excitation is specified to be a TEM wave traveling in the positive z direction in the coax, whose field components are

$$E_\rho^i = \frac{E_0}{\rho} e^{-jk_c z} , \quad H_\phi^i = \frac{E_0}{\eta_c \rho} e^{-jk_c z} , \tag{1}$$

where $k_c^2 = \omega^2 \mu_c \varepsilon_c$ and $\eta_c^2 = \mu_c/\varepsilon_c$ and where E_0 is the known complex amplitude of the TEM electric field incident upon the annular aperture. If the coax is gas-filled and the center conductor is supported by a dielectric bead, k_c and η_c are replaced by k_g and η_g, respectively. The viewpoint taken here is that the monopole can be treated as a scatterer which is illuminated by the field radiated by the coaxial aperture in the screen. This approach enables us to apply aperture and scattering theory to the present analysis and provides the basis for the formulation of a pair of coupled integral equations for the monopole-coax structure. As an aid in the derivation of equations, the formulation is partitioned into three parts: field in coaxial region, field radiated by annular aperture, field scattered by monopole.

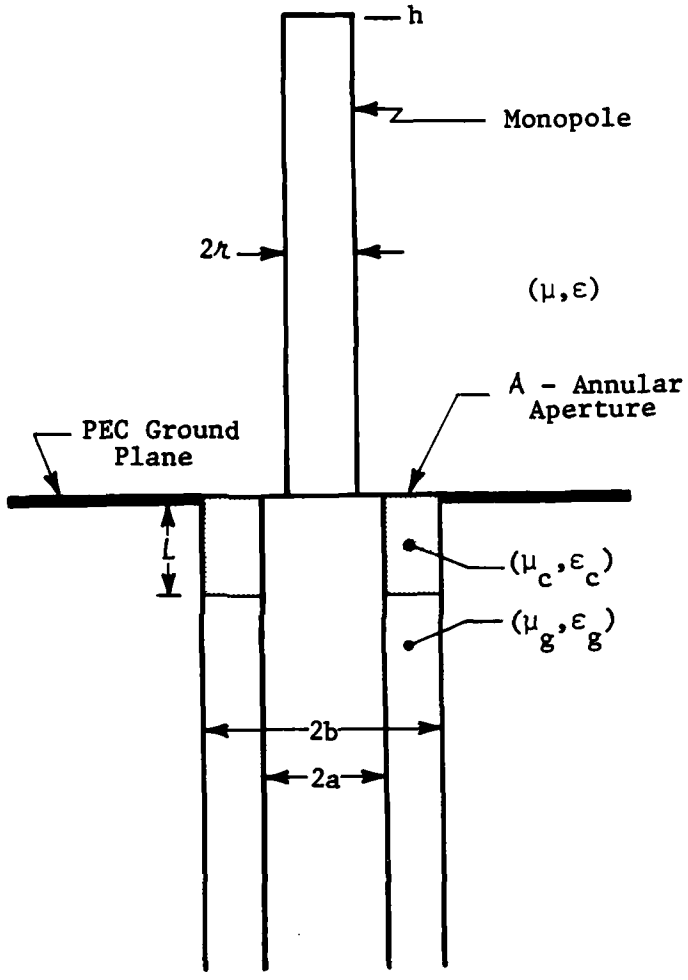

Fig. 2. Cross-section of coax-fed monopole above a ground plane (for coax filled with uniform solid dielectric, $L \to \infty$).

2. FORMULATION OF INTEGRAL EQUATIONS

Coupled integral equations are formulated in this section for the unknowns I and E_ρ^a where I is the total axial current on the monopole and E_ρ^a is the ρ component of the electric field in the annular aperture A through which the coaxial guide and monopole antenna are coupled. These integral equations are derived by requiring (i) that the ϕ component of the H-field in the coax be equal to that in the exterior region when both are evaluated in the limit as the points of observation appr .h the annular aperture and (ii) that the electric field tangential t .he monopole and to the conducting plane be zero. For this purpose t . magnetic field is expressed in the coaxial guide as a function of E_ρ^a and of the excitation and in the exterior region as a function of E_ρ^a and I.

Magnetic Field in Coaxial Guide

The magnetic field H_ϕ^{co} in the coaxial guide can be written in terms of the coax excitation of (1) and aperture field E_ρ^a as

$$H_\phi^{co}(\rho,z) = H_\phi^{sc}(\rho,z) + H_\phi^{c}(\rho,z) \tag{2a}$$

where

$$H_\phi^{c}(\rho,z) = \int_a^b E_\rho^a(\rho')G^c(\rho,z;\rho')d\rho' \tag{2b}$$

and in which

$$H_\phi^{sc}(\rho,z) = 2\frac{E_0}{\eta_c\rho}\cos k_c z \tag{3a}$$

is the so-called short-circuit magnetic field which would exist in the uniform-dielectric coax if the aperture at $z = 0$ between the coaxial guide and the exterior region were short-circuited. If the coax is gas-filled with a bead-supported center conductor, the short-circuit magnetic field in the region $-L < z < 0$ would be

$$H_\phi^{sc}(\rho,z) = 2\,\frac{E_0}{\rho}\cdot\frac{e^{jk_gL}}{\eta_g\cos k_cL + j\,\eta_c\sin k_cL}\cos k_cz,\ z\,\varepsilon(-L,0). \qquad (3b)$$

In the case of the gas-filled coax, (2a) is valid only in the bead material ($-L < z < 0$), and it is assumed that higher order modes excited at the discontinuity at $z = 0$ are vanishing small at $z = -L$. The Green's function G^c is determined by standard methods [1] to be

$$G^c(\rho,z;\rho') = -\frac{1}{\eta_c\rho\ell n\frac{b}{a}}\,e^{jk_cz}\left[\frac{1-\Gamma\,e^{-j2k_c(z+L)}}{1+\Gamma\,e^{-j2k_cL}}\right]$$

$$-\frac{k_c}{\eta_c}\,\rho'\sum_{q=1}^{\infty}\frac{1}{\chi_q N_q^2}\frac{d}{d\rho'}\Phi_q(\rho')\,\frac{d}{d\rho}\Phi_q(\rho)\,e^{j\chi_qz} \qquad (4)$$

$$z\varepsilon(-L,0)$$

where

$$\Gamma = \frac{\eta_g - \eta_c}{\eta_g + \eta_c}\ , \qquad (5)$$

where

$$\Phi_q(\rho) = N_0(k_{tq}a)\,J_0(k_{tq}\rho) - J_0(k_{tq}a)\,N_0(k_{tq}\rho)\ , \qquad (6)$$

and where

$$\chi_q = \begin{cases}\sqrt{k_c^2 - k_{tq}^2}\ , & k_{tq}^2 < k_c^2\\ -j\sqrt{k_{tq}^2 - k_c^2}\ , & k_{tq}^2 > k_c^2\end{cases} \qquad (7)$$

in which k_{tq}, $q = 1,2,\ldots$, is the q^{th} root of $\Phi_q(b) = 0$. In (6), J_ν and N_ν are the ν^{th} order Bessel and Neumann functions and the norm N_q^2 in (4) is

$$N_q^2 = \int_a^b \rho \left[\frac{d}{d\rho}\,\Phi_q(\rho)\right]^2 d\rho = \frac{b^2}{2}\left(\left[\frac{d}{d\rho}\,\Phi_q(\rho)\right]_{\rho=b}\right)^2 - \frac{2}{\pi^2}\,. \tag{8}$$

The Green's function G^c of (4) is valid for both the uniform-dielectric coax and the gas-filled coax with bead-supported center conductor; in the former case, Γ is set equal to zero in the first term of (4).

Field in Exterior Region

The magnetic field in the exterior region is determined as the sum

$$H_\phi^{ex} = H_\phi^r + H_\phi^s \tag{9}$$

where H_ϕ^r is that radiated by the annular aperture in the absence of the monopole and H_ϕ^s is that scattered by the monopole. The field incident upon the monopole is that radiated by the aperture. As an aid in deriving expressions for the exterior field, the exterior-field equivalent model of Fig. 3 is introduced. In this figure one sees that the annular aperture A at $z = 0$ is short-circuited and that an equivalent surface magnetic current of density $\underline{M} = M_\phi\hat{\underline{\phi}}$ where $M_\phi = \hat{\underline{\phi}} \cdot \left[E_\rho^a\,\hat{\underline{\rho}} \times \hat{\underline{z}}\right]$ or $M_\phi = -E_\rho^a$ is placed on the shorted annulus [2]. This model and its field are equivalent to the original structure and its field in the exterior ($z > 0$) region [2]. By image theory one arrives at the final model of Fig. 3, which is used as a guide in exterior formulations.

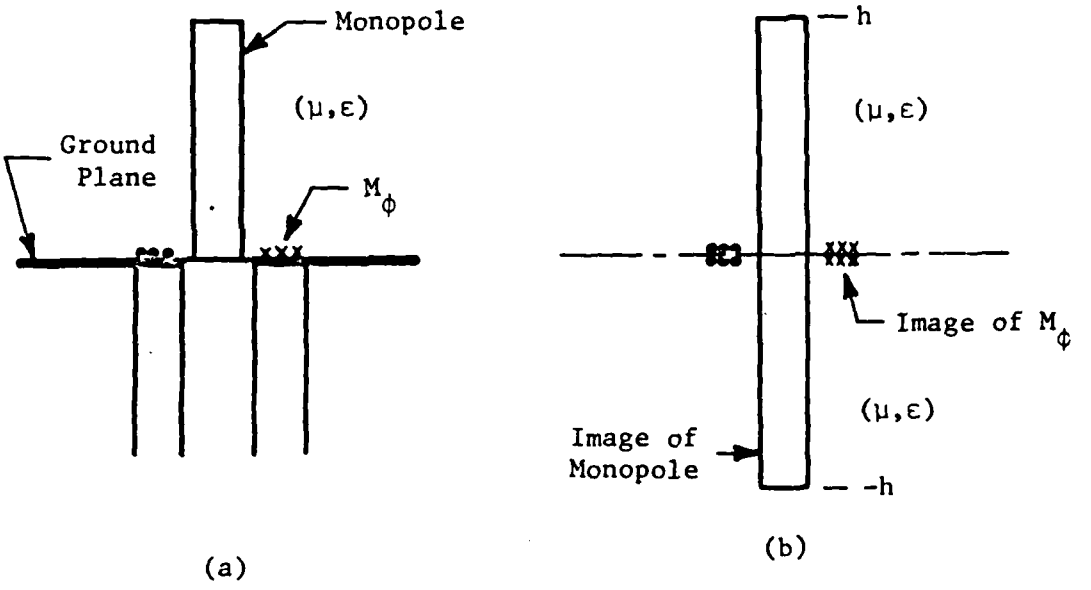

Fig. 3. Exterior-region equivalent models of coax-fed monopole.

In the absence of the monopole, the field $(\underline{E}^r, \underline{H}^r)$ due to the magnetic current is determined from

$$\underline{E}^r = -\frac{1}{\varepsilon} \nabla \times \underline{F} \tag{10a}$$

and

$$\underline{H}^r = -j \frac{\omega}{k^2} (k^2 \underline{F} + \nabla\nabla \cdot \underline{F}) \tag{10b}$$

where

$$\underline{F}(\underline{r}) = \frac{\varepsilon}{4\pi} \iint_A 2M_\phi(\rho') \hat{\underline{\phi}}' \frac{e^{-jk|\underline{r}-\underline{\rho}'|}}{|\underline{r}-\underline{\rho}'|} dS' \tag{11}$$

or where $\underline{F} = F_\phi \hat{\underline{\phi}}$ with

$$F_\phi(\rho,z) = -\frac{\varepsilon}{2\pi} \int_a^b \rho' E_\rho^a(\rho') \int_{-\pi}^{\pi} \cos\phi' \frac{e^{-jk[z^2 + R^2]^{\frac{1}{2}}}}{[z^2 + R^2]^{\frac{1}{2}}} d\phi' d\rho' \tag{12a}$$

in which $k^2 = \omega^2\mu\varepsilon$ and $\eta^2 = \mu/\varepsilon$ and

$$R^2 = [\rho^2 + \rho'^2 - 2\rho\rho'\cos\phi'] \ . \tag{12b}$$

From (10) and (12) one readily finds that the field components E_z^r and H_ϕ^r are

$$E_z^r(\rho,z) = \frac{1}{2\pi\rho} \frac{\partial}{\partial\rho} \rho \int_a^b \rho' E_\rho^a(\rho') \int_{-\pi}^{\pi} \cos\phi' \frac{e^{-jk[z^2 + R^2]^{\frac{1}{2}}}}{[z^2 + R^2]^{\frac{1}{2}}} d\phi' d\rho' \ . \tag{13}$$

and

$$H_\phi^r(\rho,z) = j \frac{1}{2\pi} \frac{k}{\eta} \int_a^b \rho' E_\rho^a(\rho') \int_{-\pi}^{\pi} \cos\phi' \frac{e^{-jk[z^2 + R^2]^{\frac{1}{2}}}}{[z^2 + R^2]^{\frac{1}{2}}} d\phi' d\rho' . \tag{14}$$

The field $(\underline{E}^s, \underline{H}^s)$ due to the total axial current I induced on the monopole can be determined from

$$\underline{E}^s = -j \frac{\omega}{k^2} (k^2 \underline{A} + \underline{\nabla\nabla} \cdot \underline{A}) \tag{15a}$$

and

$$\underline{H}^s = \frac{1}{\mu} \underline{\nabla} \times \underline{A} \tag{15b}$$

where $\underline{A}$ has only a z-component given by

$$A_z(\rho,z) = \frac{\mu}{4\pi} \int_{-h}^{h} I(z') \frac{1}{2\pi} \int_{-\pi}^{\pi} \frac{e^{-jk[(z-z')^2 + R_\ell^2]^{\frac{1}{2}}}}{[(z-z')^2 + R_\ell^2]^{\frac{1}{2}}} d\phi' dz' \tag{16}$$

in which R_ℓ^2 is R^2 of (12b) with ρ' replaced by ℓ. As is consistent with the fact that the excitation of the monopole emanating from the aperture is ϕ independent, the current on the monopole and the resulting scattered field are also ϕ independent. Expressions for the field components E_z^s and H_ϕ^s follow immediately:

$$E_z^s(\rho,z) = -j \frac{\eta}{4\pi k} \left(\frac{d^2}{dz^2} + k^2\right) \int_{-h}^{h} I(z') \frac{1}{2\pi} \int_{-\pi}^{\pi} \frac{e^{-jk[(z-z')^2 + R_\ell^2]^{\frac{1}{2}}}}{[(z-z')^2 + R_\ell^2]^{\frac{1}{2}}} d\phi' dz' \tag{17}$$

$$H_\phi^s(\rho,z) = -\frac{1}{4\pi} \frac{\partial}{\partial\rho} \int_{-h}^{h} I(z') \frac{1}{2\pi} \int_{-\pi}^{\pi} \frac{e^{-jk[(z-z')^2 + R_\ell^2]^{\frac{1}{2}}}}{[(z-z')^2 + R_\ell^2]^{\frac{1}{2}}} d\phi' dz' \,. \tag{18}$$

Integral Equations

The final integral equations for E_ρ^a and I result from enforcement of boundary and transition conditions. The boundary condition is that the total electric field tangential to the monopole and ground plane surfaces be zero. The tangential E-field on the ground plane is zero by virtue of the use of image theory in the construction of

expressions for $\underline{E}^r$ and $\underline{E}^s$ and that on the surface of the tubular monopole is made zero by enforcement of the following equation:

$$E_z^s(\mathcal{r},z) + E_z^r(\mathcal{r},z) = 0 \quad , \; z\varepsilon(-h,h) \; . \tag{19}$$

The required transition condition is that the magnetic field tangential to the annular aperture A in the exterior region and that in the coax be equal when the points of observation approach a common point in A. This condition is ensured upon enforcement of

$$\lim_{z\uparrow 0} H_\phi^{co}(\rho,z) = \lim_{z\downarrow 0} H_\phi^{ex}(\rho,z) \quad , \; \rho\varepsilon A$$

or of

$$\lim_{z\uparrow 0} H_\phi^{co}(\rho,z) = \lim_{z\downarrow 0} \left[H_\phi^r(\rho,z) + H_\phi^s(\rho,z) \right] \quad , \; \rho\varepsilon A \; . \tag{20}$$

Eqs. (19) and (20) must hold simultaneously and, upon utilization of (2), (3), and (13)-(18), they lead to the coupled integral equations below for E_ρ^a and I:

$$-j\frac{\eta}{4\pi k}\left(\frac{d^2}{dz^2}+k^2\right)\int_{-h}^{h} I(z')\, G^s(\mathcal{r},z;z')dz'$$

$$+\frac{1}{\mathcal{r}}\left[\frac{\partial}{\partial\rho}\,\rho\int_a^b \rho' E_\rho^a(\rho')\, G^a(\rho,z;\rho')d\rho'\right]_{\rho=\mathcal{r}} = 0 \; , \; z\varepsilon(-h,h) \tag{21a}$$

and

$$-\frac{1}{4\pi}\frac{\partial}{\partial\rho}\int_{-h}^{h} I(z')\, G^s(\rho,0;z')dz' + j\frac{k}{\eta}\int_a^b \rho' E_\rho^a(\rho')\, G^a(\rho,0;\rho')d\rho'$$

$$-\int_a^b E_\rho^a(\rho')\, G^c(\rho,0;\rho')d\rho' = H_\phi^{sc}(\rho,0), \; \rho\varepsilon(a,b) \tag{21b}$$

in which

$$G^s(\rho,z;z') = \frac{1}{2\pi}\int_{-\pi}^{\pi} \frac{e^{-jk[(z-z')^2 + R_\ell^2]^{\frac{1}{2}}}}{[(z-z')^2 + R_\ell^2]^{\frac{1}{2}}}\, d\phi' \tag{22a}$$

and

$$G^a(\rho,z;\rho') = \frac{1}{2\pi}\int_{-\pi}^{\pi} \cos\phi' \frac{e^{-jk[z^2 + R^2]^{\frac{1}{2}}}}{[z^2 + R^2]^{\frac{1}{2}}}\, d\phi' \ . \tag{22b}$$

For subsequent convenience, the integral equations are written below in operator form:

$$E_z^s[I;z] + E_z^r[E_\rho^a;z] = 0 \quad , \ z\varepsilon(-h,h) \tag{23a}$$

and

$$H_\phi^s[I;\rho] + H_\phi^r[E_\rho^a;\rho] - H_\phi^c[E_\rho^a;\rho] = H_\phi^{sc}(\rho,0) \quad , \ \rho\varepsilon(a,b) \ . \tag{23b}$$

I and $E_\rho^a(=-M_\phi)$can be determined by solving the coupled integral equations and from knowledge of these two quantities the radiated field and the input TEM reflection coefficient of the coaxial guide can be computed.

3. NUMERICAL SOLUTION METHOD

The integral equations for E_ρ^a and I are far too complex to be solved by any but a well-conceived numerical method. Due to the presence of G^c, one must sum an infinite series comprising terms involving derivatives of Φ_q which depends upon Bessel and Neumann functions whose arguments are determined by a solution of a transcendental equation for each q. In addition the following terms in the integral equations involve integrals whose integrands may be singular: $E_z^s(\rho,z)$, $E_z^r(\rho,z)$, $\lim_{z\uparrow 0} H_\phi^c(\rho,z)$, and $\lim_{z\downarrow 0} H_\phi^{ex}(\rho,z)$. A technique has been developed for solving numerically the integral equations and schemes to handle <u>all</u> the difficulties enumerated have been devised. This technique is described below.

The current I on the monopole and its image as well as ρE_ρ^a in the annulus are represented by linear combinations of pulses Π_n of the forms

$$I(z) = \sum_{n=1}^{N_s} I_n \Pi_n(z) \tag{24a}$$

and

$$\rho E_\rho^a(\rho) = \sum_{n=1}^{N_a} V_n \Pi_n(\rho) \tag{24b}$$

where I_n and V_n are unknown constants to be determined, N_s is the number of non-zero pulses in the interval (-h,h),and N_a is the number of pulses in the interval (a,b). The pulse functions are defined as

$$\Pi_n(\zeta) = \begin{cases} 1, & \zeta \in (\zeta_n - \Delta\zeta/2,\ \zeta_n + \Delta\zeta/2) \\ 0, & \text{otherwise} \end{cases} \tag{25}$$

where ζ_n is the pulse center and $\Delta\zeta$ is its width. On (-h,h) the n^{th} pulse center is at $z_n = -h + n\Delta z$ and the pulse width Δz has value $\Delta z = 2h/(N_s+1)$ while on (a,b) the n^{th} pulse center is at $\rho_n = a + \Delta\rho(n-\frac{1}{2})$ and the pulse width $\Delta\rho$ has value $\Delta\rho = (b-a)/N_a$. In keeping with the boundary condition $I(\pm h) = 0$, "half pulses" are placed on the subintervals $(-h,-h+\Delta z/2)$ and $(h-\Delta z/2,h)$, and their coefficients are set equal to zero. Eq. (21a) is tested [3] with triangles Λ_m, $m = 1,\ldots,N_s$, defined by

$$\Lambda_m(z) = \begin{cases} 1 - \dfrac{|z - z_m|}{\Delta z} & , \quad z\varepsilon(z_{m-1},z_{m+1}) \\ 0 & , \quad \text{otherwise} \end{cases} \tag{26}$$

to obtain

$$\sum_{n=1}^{N_s} I_n Z_{mn} + \sum_{n=1}^{N_a} V_n \Gamma_{mn}^{sa} = 0 \ , \quad m=1,2,\ldots,N_s \tag{27a}$$

where

$$Z_{mn} = + j \frac{\eta}{4\pi k} \int_{-h}^{h} \Lambda_m(z) \left(\frac{d^2}{dz^2} + k^2 \right) \int_{-h}^{h} \Pi_n(z') \, K(z-z')dz'dz \tag{27b}$$

and

$$\Gamma_{mn}^{sa} = - \frac{1}{\pi} \int_{-h}^{h} \Lambda_m(z) \left[\frac{\partial}{\partial\rho} \rho \int_{a}^{b} \Pi_n(\rho') \, G^a(\rho,z;\rho')d\rho' \right]_{\rho=\pi} dz \ . \tag{27c}$$

In (27b) $K(z-z') = G^s(\rho,z;z')$ is the exact kernel [4] of cylindrical antenna and scatterer theory. Eq. (21b) is tested with delta functions or is simply enforced at match point ρ_m located at the centers of pulses to arrive at

$$\sum_{n=1}^{N_s} I_n \Gamma_{mn}^{as} + \sum_{n=1}^{N_a} V_n [Y_{mn} - Y_{mn}^c] = H_m^{sc} \qquad (28a)$$

$$m = 1,2,\ldots,N_a$$

where $H_m^{sc} = H_\phi^{sc}(\rho_m,0)$, where $\rho_m = a + \Delta\rho(m-\frac{1}{2})$, and where

$$\Gamma_{mn}^{as} = -\frac{1}{4\pi}\left[\frac{\partial}{\partial\rho}\int_{-h}^{h} \Pi_n(z')\, G^s(\rho,0;z')dz'\right]_{\rho=\rho_m} , \qquad (28b)$$

$$Y_{mn} = j\frac{k}{\eta}\int_a^b \Pi_n(\rho')\, G^a(\rho_m,0;\rho')d\rho' , \qquad (28c)$$

and

$$Y_{mn}^c = \int_a^b \Pi_n(\rho')\frac{1}{\rho'} G^c(\rho_m,0;\rho')d\rho' . \qquad (28d)$$

In view of the properties of the pulse function Π_n of (25) and of the triangle function Λ_m of (26), Z_{mn} and Γ_{mn}^{sa} of (27) can be simplified [5 , 6] to

$$Z_{mn} = j\frac{\eta}{4\pi k\Delta z}\int_{-\Delta z/2}^{\Delta z/2}\Big\{K(z_{m+1} - z_n - \zeta) - 2[1-\tfrac{1}{2}(k\Delta z)^2]\, K(z_m - z_n - \zeta)$$

$$+ K(z_{m-1} - z_n - \zeta)\Big\}\, d\zeta \qquad (29a)$$

and

$$\Gamma_{mn}^{sa} = -\frac{1}{\hbar}\int_{-\Delta z}^{\Delta z}[1-|\zeta|/\Delta z]\left[\frac{\partial}{\partial\rho}\,\rho\int_{-\Delta\rho/2}^{\Delta\rho/2}G^{a}(\rho,\,\zeta+z_m;\,\xi+\rho_n)d\xi\right]_{\rho=\hbar}d\zeta\ . \qquad (29b)$$

Integration by parts twice and the change of variable $z' = z_n + \zeta$ are employed to transform (27b) into (29a) while the variable changes $z = z_m + \zeta$ and $\rho' = \rho_n + \xi$ are employed to transform (27c) into (29b). Also involved in the conversion from (27b) to (29a) is a very accurate approximation [5 , 6]. By making use of properties of Π_n and the variable changes mentioned above, the expressions of (28) for Γ_{mn}^{as} , Y_{mn}, and Y_{mn}^{c} can be converted to

$$\Gamma_{mn}^{as} = -\frac{1}{4\pi}\left[\frac{\partial}{\partial\rho}\int_{-\Delta z/2}^{\Delta z/2}G^{s}(\rho,0;z_n+\zeta)d\zeta\right]_{\rho=\rho_m}\ , \qquad (30a)$$

$$Y_{mn} = j\,\frac{k}{\eta}\int_{-\Delta\rho/2}^{\Delta\rho/2}G^{a}(\rho_m,0;\rho_n+\xi)d\xi\ , \qquad (30b)$$

and

$$Y_{mn}^{c} = \int_{-\Delta\rho/2}^{\Delta\rho/2}\frac{1}{\rho_n+\xi}\,G^{c}(\rho_m,0;\rho_n+\xi)d\xi\ . \qquad (30c)$$

To facilitate subsequent discussion it is convenient to express (27a) and (28a) as a single matrix equation of the form

$$\begin{bmatrix}[Z_{mn}] & [\Gamma_{mn}^{sa}]\\ [\Gamma_{mn}^{as}] & [Y_{mn}-Y_{mn}^{c}]\end{bmatrix}\begin{bmatrix}[I_n]\\ [V_n]\end{bmatrix} = \begin{bmatrix}[0]\\ [H_m^{sc}]\end{bmatrix}\ . \qquad (31)$$

Analytical/numerical procedures for computing the matrix elements from (29) and (30) are presented below.

Analytical Aids in the Numerical Evaluation of Matrix Elements

In this section are presented analytical procedures which greatly enhance the accuracy and efficiency of methods for numerical evaluation of the matrix elements of (31). In fact, without the analysis outlined below it is unlikely that sufficient accuracy of matrix element values could be attained to allow acceptable numerical solutions. Z_{mn} is omitted from the discussion below since procedures for its evaluation can be found elsewhere [4,6].

As a first step in casting Γ_{mn}^{sa} into a form suitable for computation we point out that by making use of the analysis presented in [7] one can show that Γ_{mn}^{sa} of (29b) can be reduced to

$$\Gamma_{mn}^{sa} = \int_{-\Delta z}^{\Delta z} (1 + \frac{|\zeta|}{\Delta z})[g_{m,n+\frac{1}{2}}(\zeta) - g_{m,n-\frac{1}{2}}(\zeta)]d\zeta \qquad (32a)$$

where

$$g_{m,n\pm\frac{1}{2}}(\zeta) = \frac{1}{2\pi}\int_{-\pi}^{\pi} \frac{e^{-jk_o R_{m,n\pm\frac{1}{2}}}}{R_{m,n\pm\frac{1}{2}}} d\phi' \qquad (32b)$$

and

$$R^2_{m,n\pm\frac{1}{2}} = (\zeta + z_m)^2 + r^2 + (\rho_n \pm \tfrac{1}{2}\Delta\rho)^2 - 2r(\rho_n \pm \tfrac{1}{2}\Delta\rho)\cos\phi' \quad . \qquad (32c)$$

Evaluation of (32) is essentially the same chore as evaluation of matrix elements in cylindrical antenna/scatterer theory and it can be achieved by methods developed for that purpose. In fact for $n = 1$, $g_{m,n-\frac{1}{2}} = g_{m,\frac{1}{2}}$ is a special case of the exact kernel for the circular cylinder which for $z_m = 0$ is logarithmically singular at $\zeta = 0$. Hence from the simple expression of (32), one can avail himself of any of the numerous procedures [4,6] developed for cylindrical antenna/scatterer theory to evaluate Γ^{sa}_{mn}.

A form of Γ^{as}_{mn} suitable for numerical computation is developed by noting that an interchange of differentiation and integration in (30a) is valid for $\rho \neq r$. Since the bracketed expression in (30a) is evaluated only at points $\rho = \rho_m \geq r + \frac{1}{2}\Delta\rho$, Γ^{as}_{mn} can be rewritten as

$$\Gamma^{as}_{mn} = \frac{1}{8\pi^2} \int_{-h}^{h} \int_{-\pi}^{\pi} \Pi_n(z')(1 + jkD_m)(\rho_m - r\cos\phi') \frac{e^{-jkD_m}}{D_m^3} \, d\phi' dz' \qquad (33)$$

$$\equiv \frac{1}{8\pi^2} \int_{-h}^{h} \int_{-\pi}^{\pi} \Pi_n(z') \; I_{as} \; d\phi' dz'$$

where

$$D_m = [\rho_m^2 + r^2 - 2\rho_m r \cos\phi' + z'^2]^{\frac{1}{2}}.$$

The integrand in (33) is bounded and one can evaluate the integral numerically. Because of the small size of the coax aperture, however, the observation point may be quite near the cylinder surface relative to the length of a source segment on the cylinder. Thus the integrand of (33) may be very highly peaked for the cylinder

source segment in which $|z'| < \Delta z/2$. To facilitate evaluation of (33) in this case the integral is expressed in a form more appropriate for numerical calculations. We note that

$$I_{as} \xrightarrow[kD_m \to 0]{} \left(\frac{1}{D_m^3} + \frac{k^2}{2D_m}\right)(\rho_m - r\cos\phi') \equiv I'_{as} \quad . \tag{34}$$

Thus when $n = (N_s+1)/2$, Γ_{mn}^{as} is expressed as

$$\Gamma_{mn}^{as} = \frac{1}{8\pi^2}\int_{\frac{-\Delta z}{2}}^{\frac{\Delta z}{2}}\int_{-\pi}^{\pi}(I_{as} - I'_{as})d\phi'dz' + \frac{1}{8\pi^2}\int_{\frac{-\Delta z}{2}}^{\frac{\Delta z}{2}}\int_{-\pi}^{\pi} I'_{as}\, d\phi'dz' \quad . \tag{35}$$

The highly peaked behavior of the integrand in (33) is then localized to the integrand of the last integral in (35). Furthermore, integration with respect to the variable z' can be performed analytically on I'_{as} to yield

$$\frac{1}{8\pi^2}\int_{-\pi}^{\pi}\int_{\frac{-\Delta z}{2}}^{\frac{\Delta z}{2}} I'_{as}dz'd\phi' = \frac{1}{8\pi^2}\int_{-\pi}^{\pi} I_{as}^{1'}\, d\phi' + \frac{1}{8\pi^2}\int_{-\pi}^{\pi} I_{as}^{2'}\, d\phi' \tag{36}$$

where

$$I_{as}^{1'} = \frac{\Delta z[(\rho_m - r) + r(1-\cos\phi')]}{[(\rho_m - r)^2 + 2\rho_m r(1-\cos\phi')][(\rho_m - r)^2 + 2\rho_m r(1-\cos\phi') + (\frac{\Delta z}{2})^2]^{\frac{1}{2}}} \tag{37a}$$

$$I_{as}^{2'} = k^2(\rho_m - r\cos\phi')\left\{\ell n\left[\frac{\Delta z}{2} + [\rho_m^2 + r^2 - 2\rho_m r\cos\phi' + (\frac{\Delta z}{2})^2]^{\frac{1}{2}}\right] - \frac{1}{2}\ell n(\rho_m^2 + r^2 - 2\rho_m r\cos\phi')\right\} \quad . \tag{37b}$$

The integrand $I_{as}^{2'}$ is slowly varying with respect to ϕ' and can be evaluated numerically. The integrand $I_{as}^{1'}$, however, is still highly peaked near $\phi' = 0$. We therefore subtract the small argument behavior of $I_{as}^{1'}$ under the integral sign and add it to the expression for Γ_{mn}^{as} as a separate integral, so that Γ_{mn}^{as} is finally given by

$$\Gamma_{mn}^{as} = \frac{1}{8\pi^2} \int_{\frac{-\Delta z}{2}}^{\frac{\Delta z}{2}} \int_{-\pi}^{\pi} (I_{as} - I'_{as}) d\phi' dz'$$

$$+ \frac{1}{8\pi^2} \int_{-\pi}^{\pi} (I_{as}^{1'} - I_{as}^{1''}) d\phi' + \frac{1}{8\pi^2} \int_{-\pi}^{\pi} I_{as}^{2'} d\phi'$$

$$+ \frac{1}{8\pi^2} \int_{-\pi}^{\pi} I_{as}^{1''} d\phi' \quad , \; n = (N_s+1)/2 \tag{38}$$

where I_{as}, I'_{as}, $I_{as}^{1'}$, and $I_{as}^{2'}$ are defined in (33)-(37) and where

$$I_{as}^{1''} = \frac{\Delta z[(\rho_m - r) + \frac{1}{2} r\phi'^2]}{[(\rho_m - r)^2 + (\frac{\Delta z}{2})^2]^{\frac{1}{2}}[(\rho_m - r)^2 + \rho_m r\phi'^2]} \tag{39a}$$

$$\int_{-\pi}^{\pi} I_{as}^{1''} \, d\phi' = \frac{\Delta z}{\rho_m[(\rho_m - r)^2 + (\frac{\Delta z}{2})^2]^{\frac{1}{2}}} \left\{ \pi + \frac{\rho_m + r}{\sqrt{\rho_m r}} \tan^{-1}\left(\frac{\pi\sqrt{\rho_m r}}{\rho_m - r} \right) \right\} \tag{39b}$$

For $n \neq (N_s+1)/2$, of course, Γ_{mn}^{as} may be evaluated directly from (33) via numerical integration.

To cast Y_{mn} of (30b) into a form amenable to numerical computation, one first observes from (22b) that the integrand of G^a is unbounded for $m = n$ and that it can be sharply peaked for other combinations of m and n. Thus Y_{mn} must be computed with great care. To this end, we modify the form of this integrand by adding and subtracting $1/R_{mn}$ to obtain

$$\frac{\cos\phi' \, e^{-jkR_{mn}}}{R_{mn}} = \frac{\cos\phi' \, e^{-jkR_{mn}} - 1}{R_{mn}} + \frac{1}{R_{mn}} \tag{40a}$$

where

$$R_{mn}^2 = \rho_m^2 + (\rho_n+\xi)^2 - 2\rho_m(\rho_n+\xi)\cos\phi' \, . \tag{40b}$$

The unboundedness is confined to the second term of (40a) while its first is very slowly varying and can be integrated numerically with ease. Furthermore, the integral over $(-\pi,\pi)$ of the second term can be expressed as

$$\int_{-\pi}^{\pi} \frac{1}{R_{mn}} \, d\phi' = \frac{4}{(\rho_m+\rho_n+\xi)} \int_0^{\pi/2} \frac{1}{\sqrt{1-\beta_{mn}^2 \sin^2\theta}} \, d\theta \tag{41a}$$

$$= \frac{4}{(\rho_m+\rho_n+\xi)} K(\beta_{mn}) \tag{41b}$$

where K is observed to be the complete elliptic integral of the first kind [8] and where

$$\beta_{mn}^2 = 4 \frac{\rho_m(\rho_n+\xi)}{[\rho_m+\rho_n+\xi]^2} \, . \tag{41c}$$

In view of the above, Y_{mn} of (30b) becomes

$$Y_{mn} = j\frac{k}{\eta\pi}\int_{-\Delta\rho/2}^{\Delta\rho/2}\left\{\int_0^{\pi}\left(\frac{\cos\phi'\, e^{-jkR_{mn}} - 1}{R_{mn}}\right)d\phi' + \frac{2}{(\rho_m+\rho_n+\xi)}K(\beta_{mn})\right\}d\xi. \tag{42}$$

When $m=n$, K is unbounded for $\xi\to 0$ but, fortunately, the small argument form of K can be integrated. That is,

$$\frac{2}{(2\rho_n+\xi)}K(\beta_{nn}) \xrightarrow[\xi\to 0]{} -\frac{1}{\rho_n}\ln\left(\frac{|\xi|}{8\rho_n}\right) \tag{43}$$

and

$$-\frac{1}{\rho_n}\int_{-\Delta\rho/2}^{\Delta\rho/2}\ln\left(\frac{|\xi|}{8\rho_n}\right)d\xi = \frac{\Delta\rho}{\rho_n}\left[1-\ln\left(\frac{\Delta\rho}{16\rho_n}\right)\right]. \tag{44}$$

Hence, Y_{nn} is

$$\begin{aligned} Y_{nn} = j\frac{k}{\eta\pi}\Bigg\{ & \frac{\Delta\rho}{\rho_n}\left[1-\ln\left(\frac{\Delta\rho}{16\rho_n}\right)\right] \\ & + \int_{-\Delta\rho/2}^{\Delta\rho/2}\left[\frac{2}{(2\rho_n+\xi)}K(\beta_{nn}) + \frac{1}{\rho_n}\ln\left(\frac{|\xi|}{8\rho_n}\right)\right]d\xi \\ & + \int_{-\Delta\rho/2}^{\Delta\rho/2}\int_0^{\pi}\left\{\frac{\cos\phi'\, e^{-jkR_{nn}} - 1}{R_{nn}}\right\}d\phi'd\xi\Bigg\}. \end{aligned} \tag{45}$$

The unbounded part of the elliptic integral is added to and subtracted from the integrand of (42). The integral of the added term becomes the first term of (45) while the subtracted term remains in the integrand of the first integral of (45). Therefore, both integrals of (45) have very slowly varying integrands and can be integrated numerically with ease.

The integration indicated in (30c) can be performed analytically and, as a result, Y^c_{mn} becomes

$$Y^c_{mn} = -\frac{1}{\eta_c \ln\frac{b}{a}} \frac{1}{\rho_m} \ln\left(\frac{\rho_{n+\frac{1}{2}}}{\rho_{n-\frac{1}{2}}}\right)\left[\frac{1 - \Gamma e^{-j2k_c L}}{1 + \Gamma e^{-j2k_c L}}\right]$$

$$- \frac{k_c}{\eta_c} \sum_{q=1}^{\infty} \frac{1}{\chi_q N_q^2} \frac{d}{d\rho} \Phi_q(\rho_m)\left[\Phi_q(\rho_{n+\frac{1}{2}}) - \Phi_q(\rho_{n-\frac{1}{2}})\right] \quad (46)$$

in which $\rho_{n+\frac{1}{2}} = a + n\Delta\rho$ and $\rho_{n-\frac{1}{2}} = a + \Delta\rho(n-1)$ and in which $\frac{d}{d\rho}\Phi_q(\rho_m)$ means $\left[\frac{d}{d\rho}\Phi_q(\rho)\right]_{\rho=\rho_m}$.

The series in Y^c_{mn} must be summed efficiently if the numerical procedure described here is to be practicable. This is particularly true in regard to Y^c_{mn} because of the need to solve a transcendental equation to determine the transverse eigenvalue k_{tq} of (6) prior to the computation of each series term. To this end Kummer's transformation [9] is used to accelerate convergence. To employ this technique, one determines the q^{th} term for large q of his series and then finds another series with known sum and the same large-index q^{th} term. Even though Kummer's transformation is applied to the series of the present problem under the condition that the guide is below cutoff of the higher-order modes, $k^2 < k_{tq}^2$, which is the case of major practical interest, the procedure is immediately extendable to the cases in which higher-order modes do propagate.

One can show readily that

$$k_{tq} \xrightarrow[q\to\infty]{} \frac{q\pi}{b-a} \quad (47a)$$

and subsequently that

$$\frac{1}{\chi_q N_q^2}\frac{d}{d\rho}\,\Phi_q(\rho_m)\;\Phi_q(\rho_{n\pm\frac{1}{2}}) \xrightarrow[q\to\infty]{} C_{mn\pm\frac{1}{2}}\left\{\frac{\sin q\;\theta_{mn\pm\frac{1}{2}}}{q^2}-\frac{\sin q\;\Omega_{mn\pm\frac{1}{2}}}{q^2}\right\} \tag{47b}$$

where

$$C_{mn\pm\frac{1}{2}} = j\,\frac{1}{\pi^2}\,\frac{b-a}{\sqrt{\rho_m\;\rho_{n\pm\frac{1}{2}}}} = j\,\frac{1}{\pi^2}\,\frac{b-a}{\sqrt{(a+\Delta\rho[m-\frac{1}{2}])\,(a+\Delta\rho[(n-\frac{1}{2})\pm\frac{1}{2}])}}\;, \tag{48a}$$

$$\theta_{mn\pm\frac{1}{2}} = \frac{\pi}{b-a}\;(\rho_m+\rho_{n\pm\frac{1}{2}}-2a) = \frac{\pi\Delta\rho}{b-a}\;[(m+n-1)\pm\tfrac{1}{2}]\;, \tag{48b}$$

and

$$\Omega_{mn\pm\frac{1}{2}} = \frac{\pi}{b-a}\;(\rho_m-\rho_{n\pm\frac{1}{2}}) = \frac{\pi\Delta\rho}{b-a}\;[(m-n)\mp\tfrac{1}{2})]\;. \tag{48c}$$

In [10] the series below and its closed-form sum are listed:

$$\sum_{q=2}^{\infty} S_q(\alpha) = \delta(\alpha),\quad 0<\alpha<2\pi \tag{49a}$$

where

$$S_q(\alpha) = \frac{\sin q\alpha}{q^2-1} \tag{49b}$$

and

$$\delta(\alpha) = \left[\frac{1}{4}-\ell n(2\sin\frac{\alpha}{2})\right]\sin\alpha,\quad 0<\alpha<2\pi\;. \tag{49c}$$

Notice that, apart from the factor $C_{mn\pm\frac{1}{2}}$, S_q exhibits the form of the right side of (47b) when $q\to\infty$. Applying Kummer's transformation to the series in Y^c_{mn}, one arrives at

$$Y^c_{mn} = -\frac{1}{\eta_c \ln\frac{b}{a}} \frac{1}{\rho_m} \ln\left(\frac{\rho_{n+\frac{1}{2}}}{\rho_{n-\frac{1}{2}}}\right)\left[\frac{1 - \Gamma\, e^{-j2k_cL}}{1 + \Gamma\, e^{-j2k_cL}}\right]$$

$$- \frac{k_c}{\eta_c \chi_1 N_1^2} \frac{d}{d\rho} \Phi_1(\rho_m)\left[\Phi_1(\rho_{n+\frac{1}{2}}) - \Phi_1(\rho_{n-\frac{1}{2}})\right]$$

$$- \frac{k_c}{\eta_c} \sum_{q=2}^{\infty} \left\{\frac{1}{\chi_q N_q^2} \frac{d}{d\rho} \Phi_q(\rho_m)\left[\Phi_q(\rho_{n+\frac{1}{2}}) - \Phi_q(\rho_{n-\frac{1}{2}})\right]\right.$$

$$- C_{mn+\frac{1}{2}}\left[S_q(\theta_{mn+\frac{1}{2}}) - S_q(\Omega_{mn+\frac{1}{2}})\right]$$

$$\left. + C_{mn-\frac{1}{2}}\left[S_q(\theta_{mn-\frac{1}{2}}) - S_q(\Omega_{mn-\frac{1}{2}})\right]\right\}$$

$$- \frac{k_c}{\eta_c} C_{mn+\frac{1}{2}}\left[\delta(\theta_{mn+\frac{1}{2}}) - \frac{\Omega_{mn+\frac{1}{2}}}{|\Omega_{mn+\frac{1}{2}}|}\delta(|\Omega_{mn+\frac{1}{2}}|)\right]$$

$$+ \frac{k_c}{\eta_c} C_{mn-\frac{1}{2}}\left[\delta(\theta_{mn-\frac{1}{2}}) - \frac{\Omega_{mn-\frac{1}{2}}}{|\Omega_{mn-\frac{1}{2}}|}\delta(|\Omega_{mn-\frac{1}{2}}|)\right] \qquad (50)$$

which converges in very few terms. Absolute values are used above because $\Omega_{mn+\frac{1}{2}}$ can be negative and, as indicated, (49c) is valid only for $0<\alpha<2\pi$. Since, for $\alpha<0$, $\sin\alpha = -\sin|\alpha|$, we can write

$$\sin\alpha = \frac{\alpha}{|\alpha|} \sin|\alpha| \qquad \text{for all } \alpha \ . \qquad (51)$$

This can be used to advantage to rewrite (49) as

$$\sum_{q=2}^{\infty} \frac{\sin q\,\alpha}{q^2-1} = \frac{\alpha}{|\alpha|} \sum_{q=2}^{\infty} \frac{\sin q\,|\alpha|}{q^2-1} = \frac{\alpha}{|\alpha|} \left[\frac{1}{4} - \ln(2 \sin \frac{|\alpha|}{2})\right] \sin|\alpha|$$

$$\text{for } -2\pi<\alpha<2\pi \qquad (52a)$$

or

$$\sum_{q=2}^{\infty} S_q(\alpha) = \frac{\alpha}{|\alpha|} \left[\frac{1}{4} - \ln(2 \sin \frac{|\alpha|}{2})\right] \sin\,|\alpha|, \quad -2\pi<\alpha<2\pi. \qquad (52b)$$

4. SAMPLE NUMERICAL RESULTS

In this section are included sample numerical results obtained from a computer program implementing the techniques developed in Section 2. In Figs. 4, 5, and 6 are shown current distributions and aperture field distributions for coax-fed monopoles above ground plane with the shape factors Ω = 8.54, 9.34, and 9.92, respectively, where $\Omega = 2 \ln (2h/\mathcal{A})$. The monopoles reside in air and have radii $\mathcal{A}$ = 3.175 mm, and equal to the radius a of the inner conductor of the air-filled coaxial line with b/a = 3. The operating frequency is f = 663 MHz. The computed current distributions, which are normalized in each case to the voltage in the aperture V^a, are compared with the experimental data (shown by dots) obtained by Mack [11]. The agreement is seen to be very good. Although no measured data are available to corroborate the computed aperture field distributions, it is seen that they exhibit the expected behavior near the inner and outer conductors of the coax.

In Figs. 7 and 8 are shown computed results for a very thick monopole (Ω = 2.77) immersed in fresh water (ε_r = 81, σ = 0) and sea water (ε_r = 81, σ = 4 S/m), respectively, and driven by an air-filled coaxial line. The other parameters are $\mathcal{A}$ = a = 2.78 cm, b/a = 3, and f = 300 MHz. It is observed that in the lossy water case the monopole current decays rapidly away from the driving point. Also, the driving-point admittance is much higher in this case than in the case of fresh water.

$$a/\lambda = a/\lambda = 7.022 \times 10^{-3}$$

$$b/a = 3$$

$$h/\lambda = 1/4$$

$$\varepsilon = \varepsilon_c = \varepsilon_g = \varepsilon_0$$

$$\mu = \mu_c = \mu_g = \mu_0$$

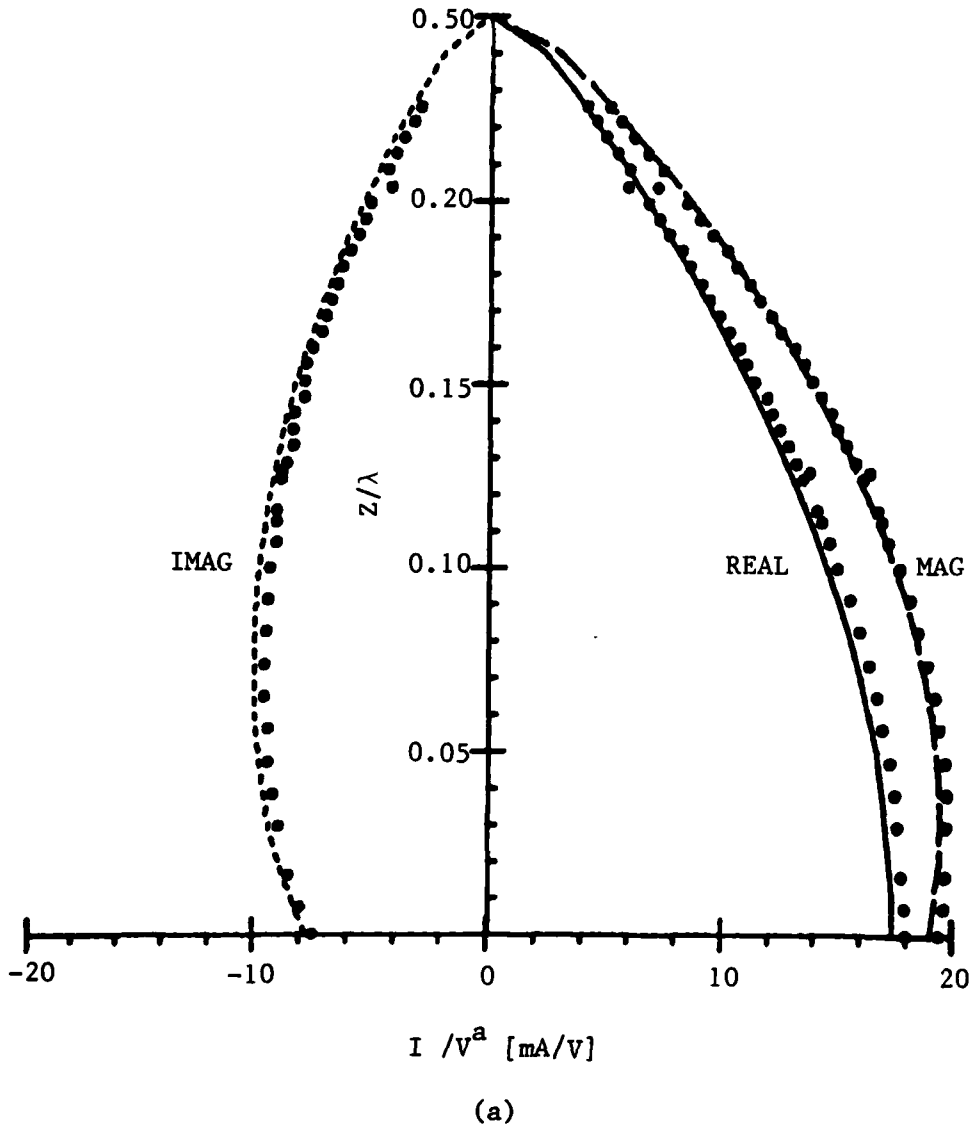

(a)

Fig. 4. Current and aperture electric field for one-quarter wavelength coax-fed monopole in air (——computed, ...measured). (a) monopole current, (b) aperture electric field.

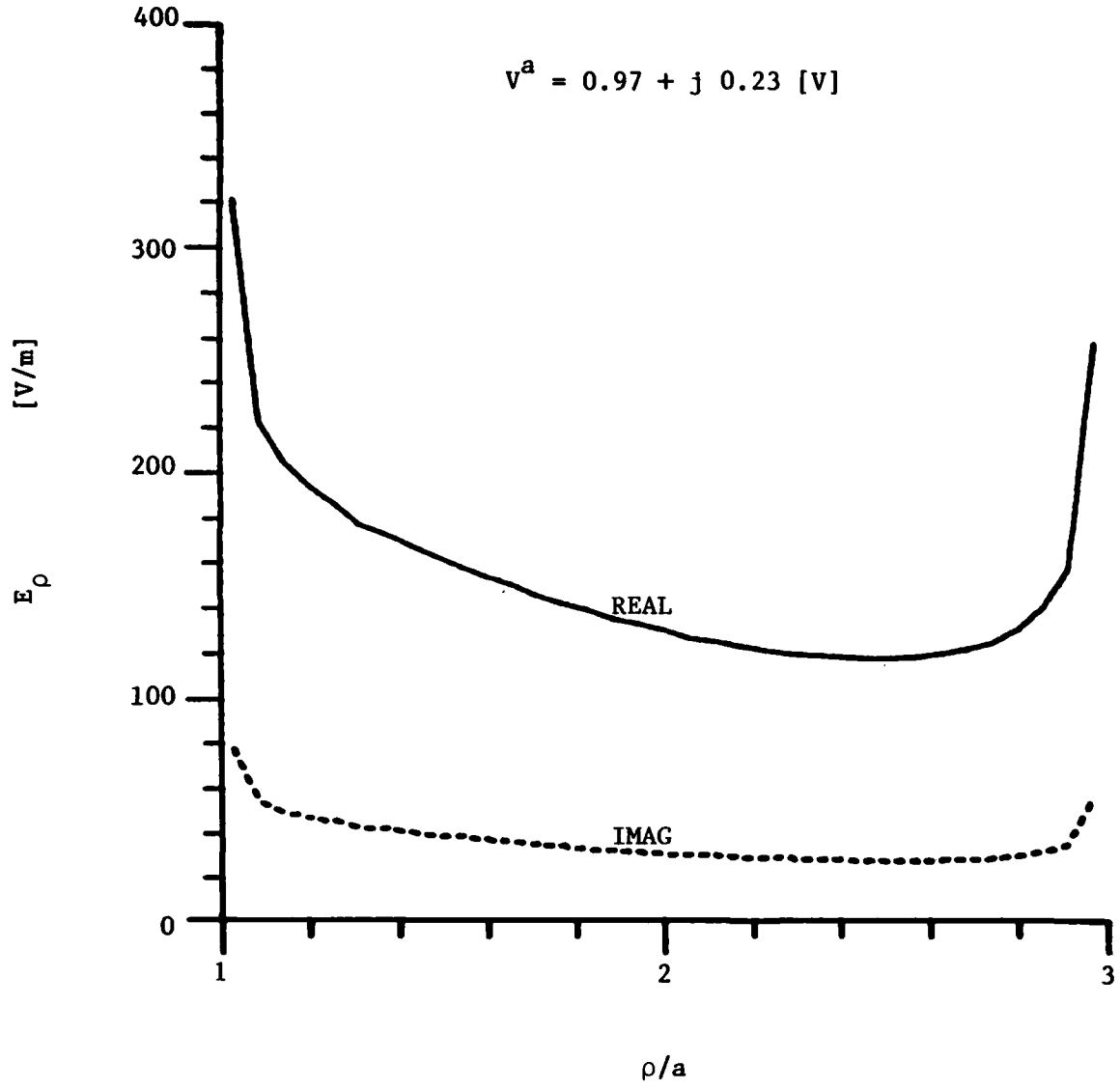

(b)

$$\mathcal{A}/\lambda = a/\lambda = 7.022 \times 10^{-3}$$

$$b/a = 3$$

$$h/\lambda = 3/8$$

$$\varepsilon = \varepsilon_c = \varepsilon_g = \varepsilon_0$$

$$\mu = \mu_c = \mu_g = \mu_0$$

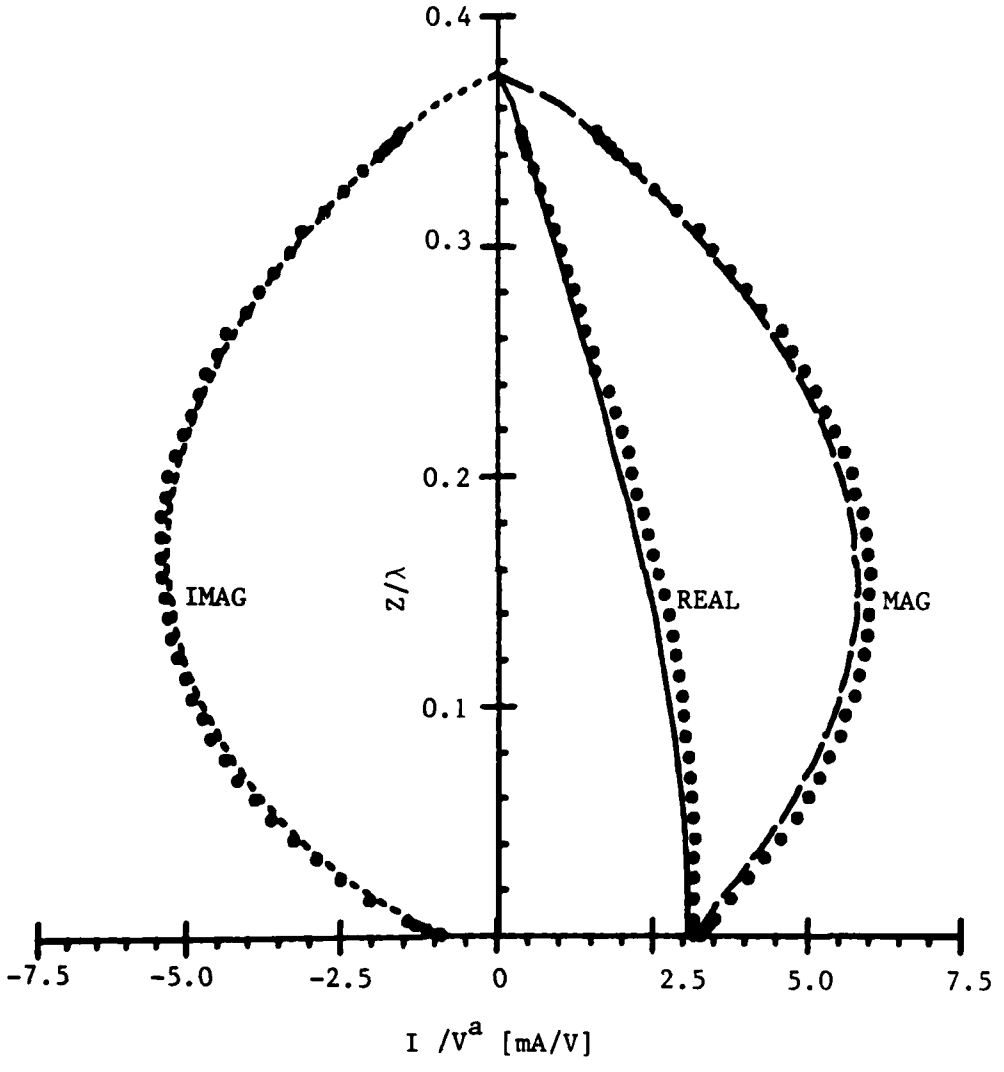

(a)

Fig. 5. Current and aperture electric field for three-eights wavelength coax-fed monopole in air (——computed,...measured). (a) monopole current, (b) aperture electric field.

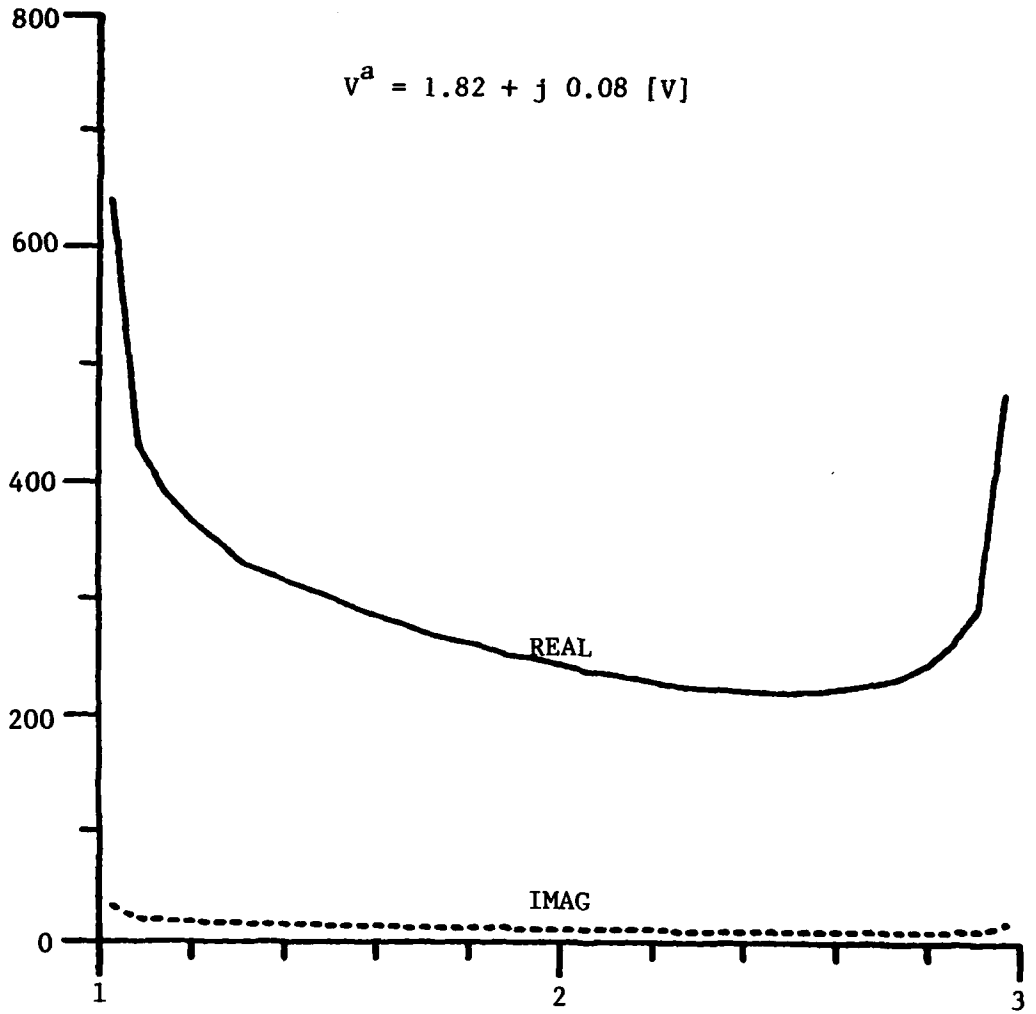

(b)

$$\hbar/\lambda = a/\lambda = 7.022 \times 10^{-3}$$

$$b/a = 3$$

$$h/\lambda = 1/2$$

$$\varepsilon = \varepsilon_c = \varepsilon_g = \varepsilon_0$$

$$\mu = \mu_c = \mu_g = \mu_0$$

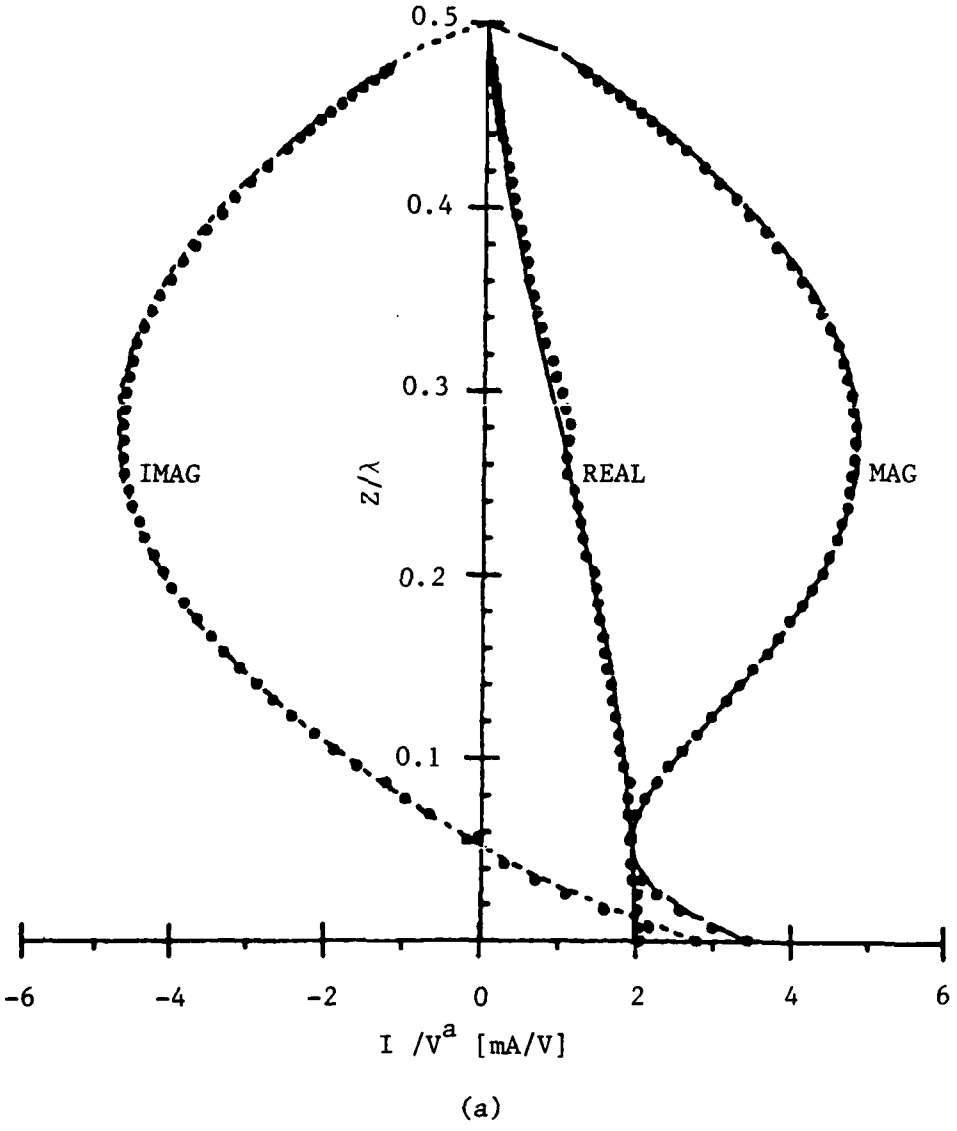

(a)

Fig. 6. Current and aperture electric field for one-half wavelength coax-fed monopole in air (——computed, ...measured). (a) monopole current, (b) aperture electric field.

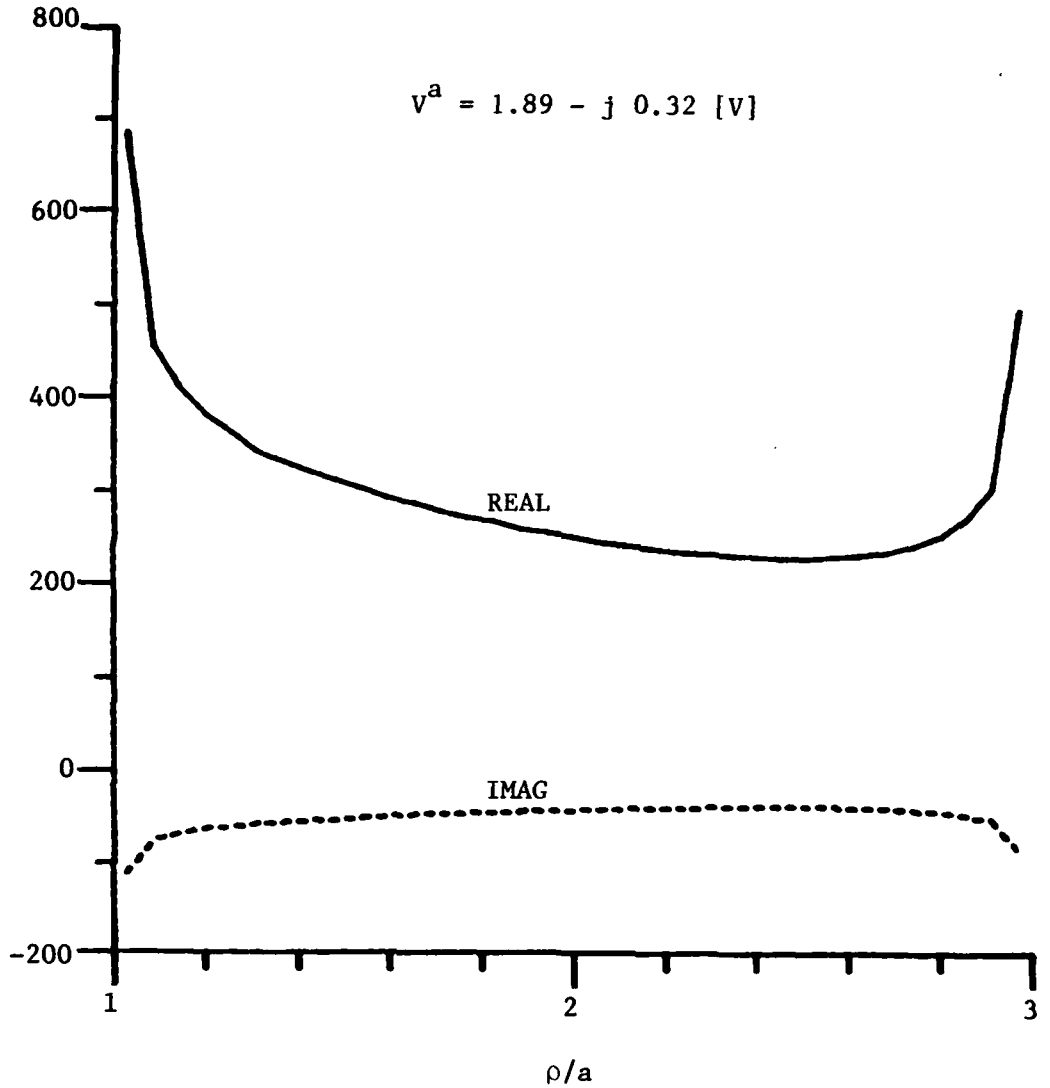

(b)

$$\kappa/\lambda = a/\lambda = 1/4$$

$$b/a = 3$$

$$h/\lambda = 1/2$$

$$\varepsilon = 81\ \varepsilon_0$$

$$\varepsilon_c = \varepsilon_g = \varepsilon_0$$

$$\mu = \mu_c = \mu_g = \mu_0$$

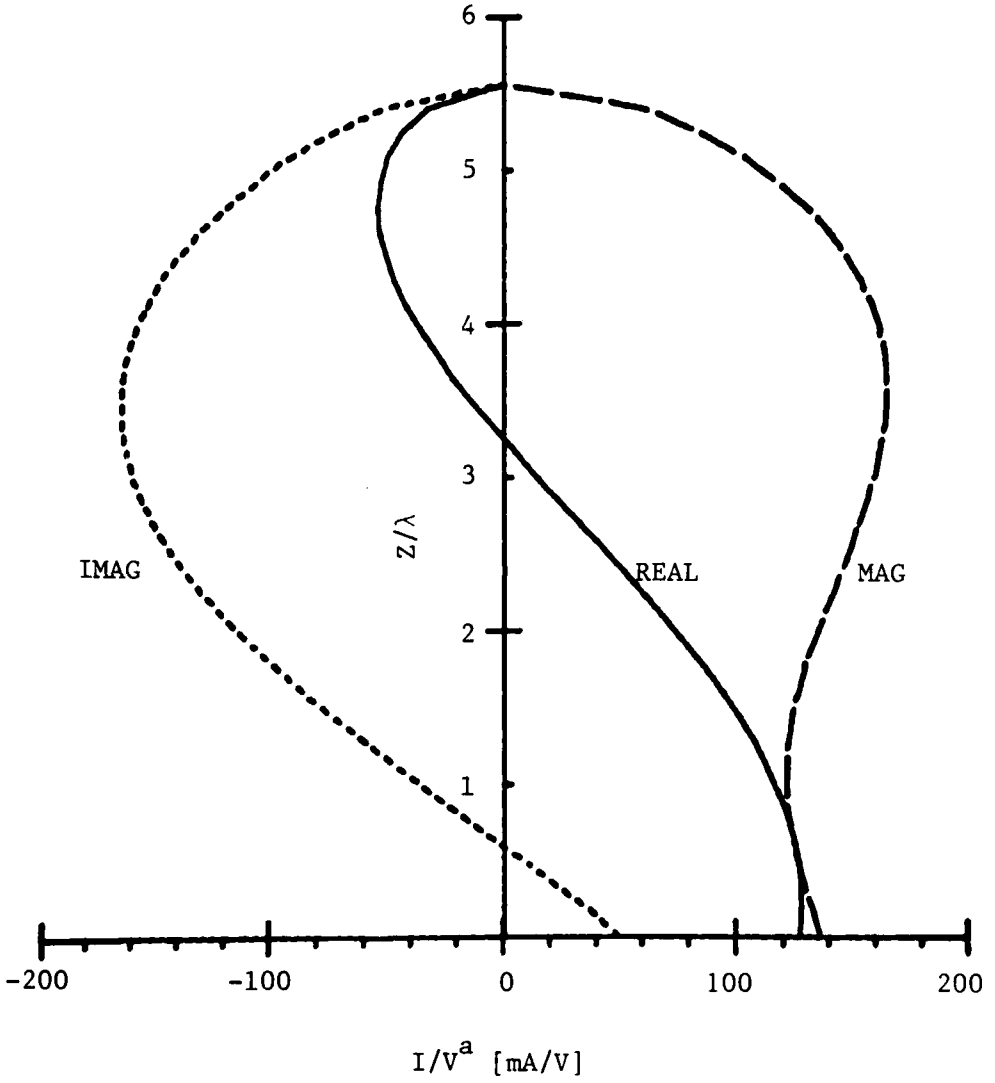

(a)

Fig. 7. Current and aperture electric field for coax-fed monopole in tap water. (a) monopole current, (b) aperture electric field.

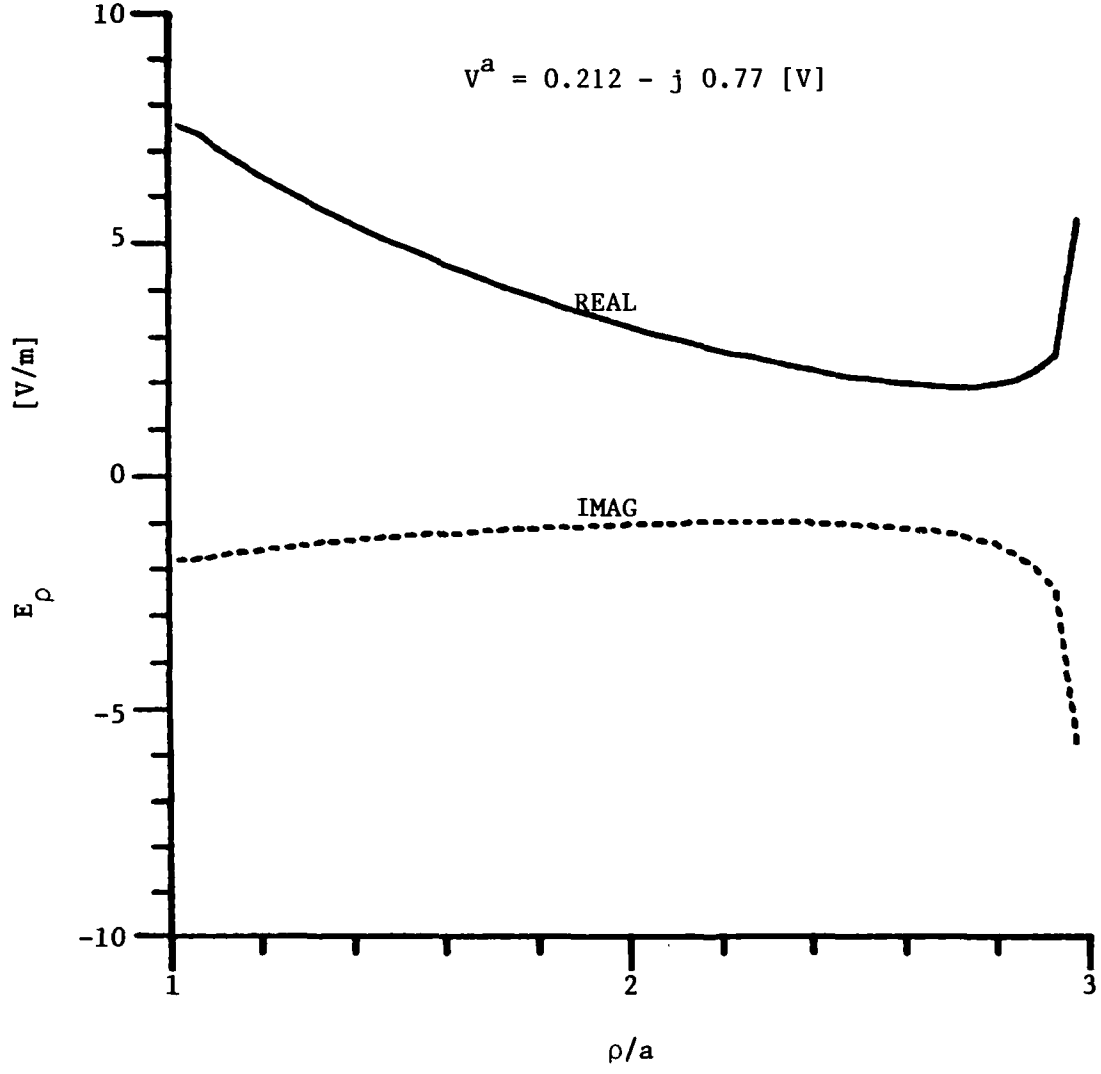

(b)

$$\mathcal{A} = a = 2.78 \text{ cm}$$

$$b/a = 3$$

$$h = 5.56 \text{ cm}$$

$$f = 300 \text{ MHz}$$

$$\varepsilon = 81\,\varepsilon_0 - j\,4/\omega$$

$$\varepsilon_c = \varepsilon_g = \varepsilon_0$$

$$\mu = \mu_c = \mu_g = \mu_0$$

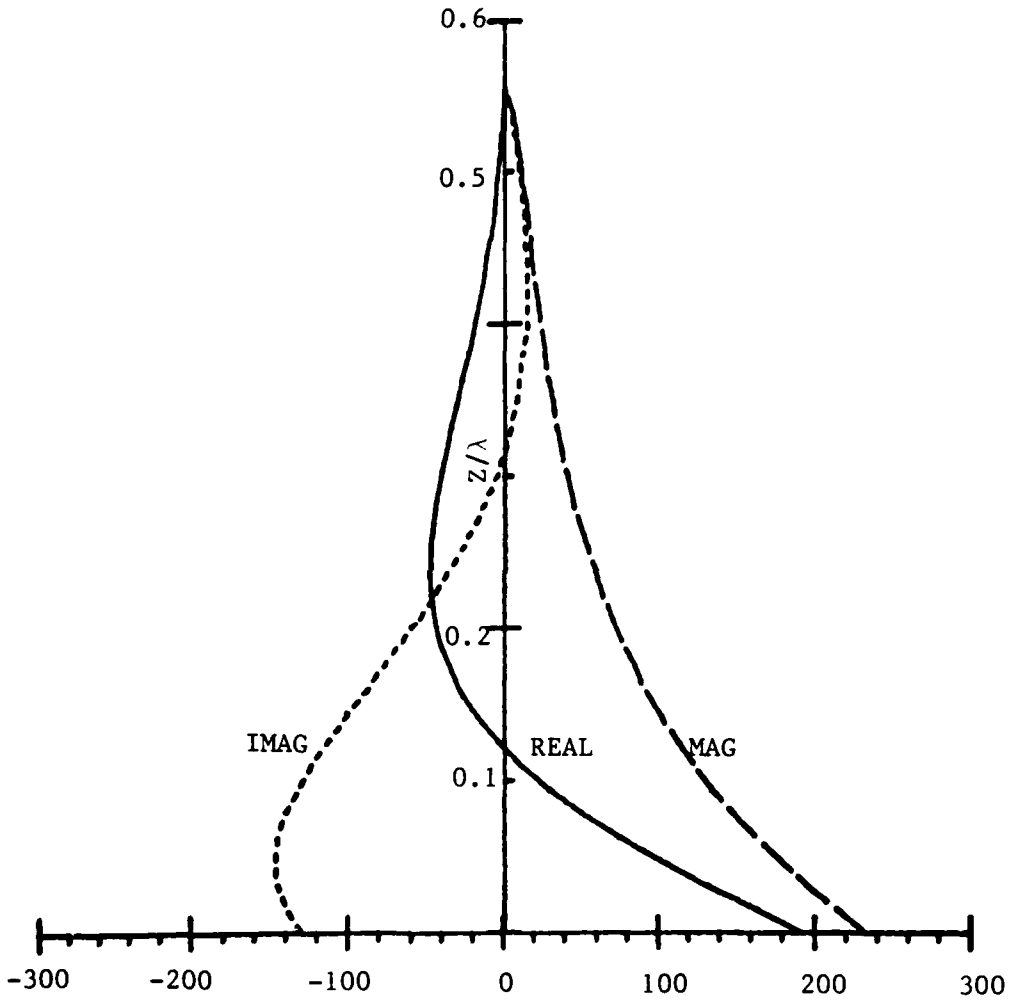

(a)

Fig. 8. Current and aperture electric field for coax-fed monopole in lossy medium. (a) monopole current, (b) aperture electric field.

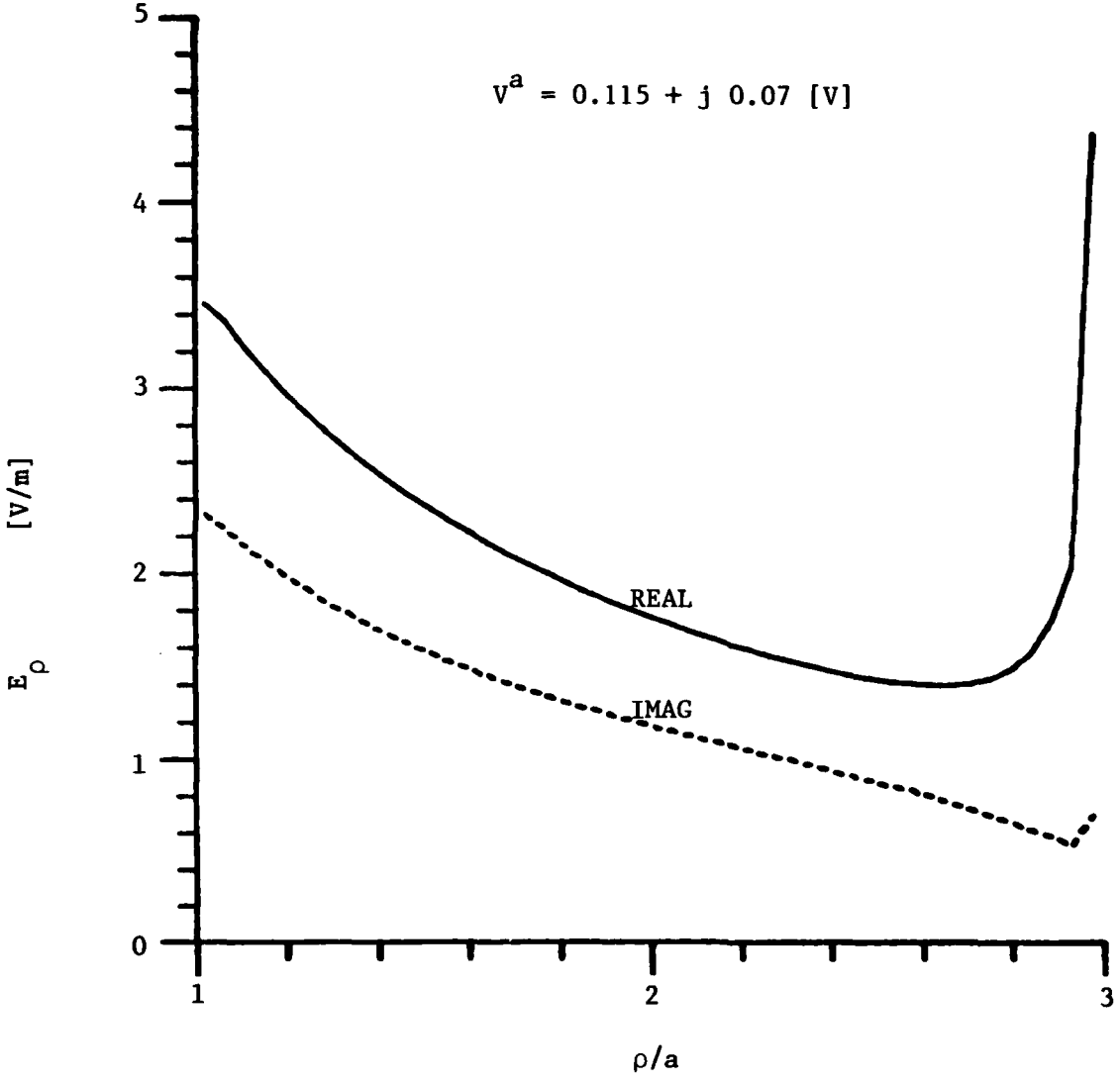

(b)

Finally, in Fig. 9 is shown a plot versus frequency of the driving-point admittance (normalized to Y_0 = 0.029 S) of a coax-fed monopole of radius $\mathcal{A}$ = a = 0.31 cm and height h = 1.65 cm immersed in tap water (ε_r = 82, σ = 0.11 S/m).* The driving coaxial line has b/a = 2.29 and is air-filled except for a teflon bead (ε_r = 2.1) of length L = 0.99 cm at the ground plane. The computed results (shown by boxes) are compared with experimental data (shown by pluses) obtained by Harrison and Butler [12]. Although the computed conductance is generally larger than that determined experimentally, there is excellent agreement at peak values. A major difference of some concern is that the computed frequency for zero phase angle does not coincide with the computed frequency for peak conductance. In the experiment, peak conductance and zero phase angle occurred at approximately the same frequency. The wavelength in the water at 500 MHz is approximately 2.6 inches, and the monopole height is approximately 0.65 inch while its radius is 0.25 inch. Fabrication of an antenna of these dimensions to close tolerances relative to the above-mentioned wavelength is difficult, especially so since the monopole must be suitable for underwater operation. Construction inaccuracy is likely a contributor to the failure of computed and measured data to agree better.

*Actually ε_r and σ are slightly frequency dependent over the frequency range under consideration; these representative values are used in the computations for convenience.

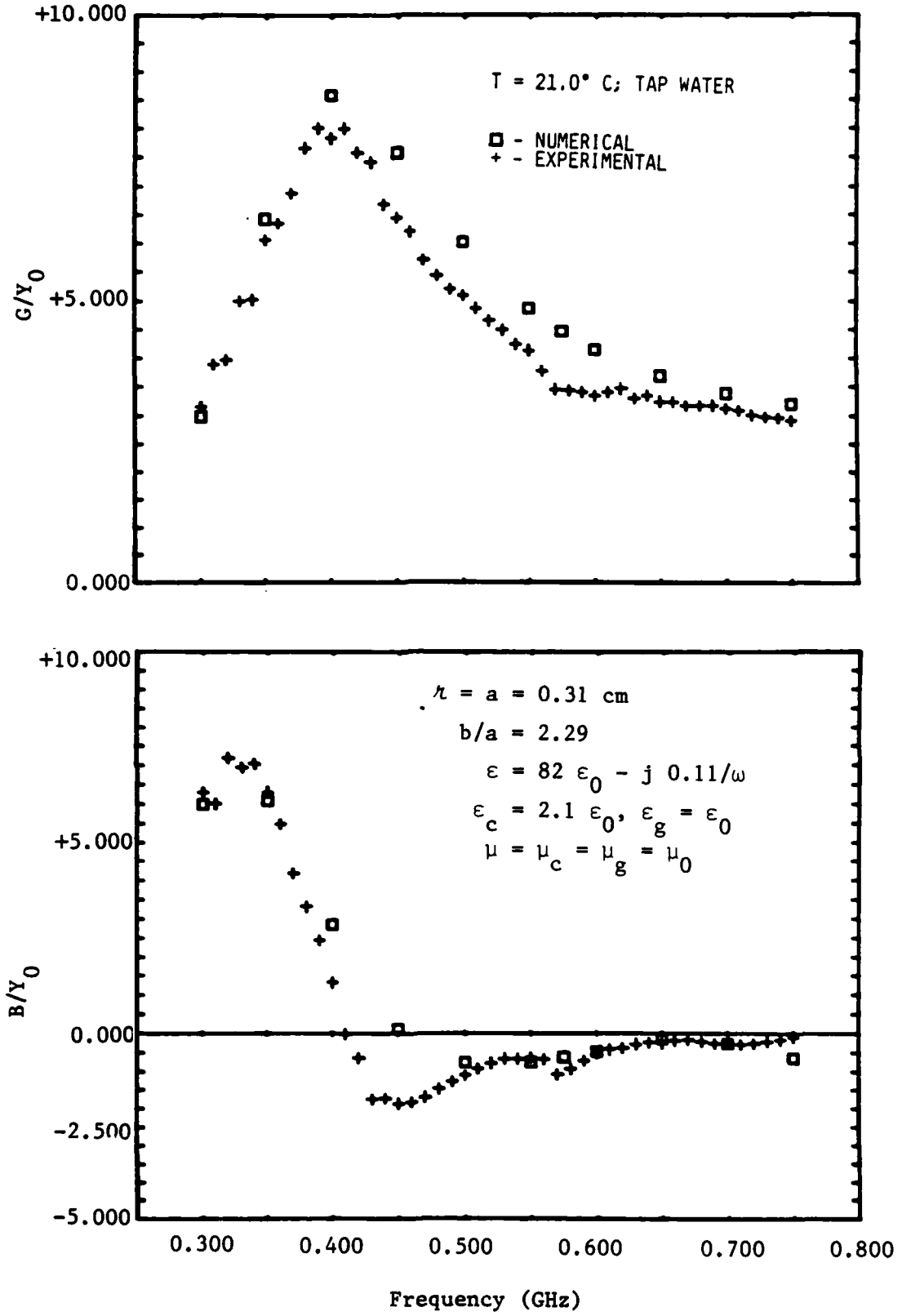

Fig. 9. Normalized (with respect to Y_0(=0.029 S)) admittance of coax-fed monopole in water.

REFERENCES

1. Harrison, M.G., and C.M. Butler, "An analytical and experimental investigation of planar discontinuities in coaxial waveguides," Technical Report AFWL-TR-79-187, Air Force Weapons Laboratory, Kirtland Air Force Base, NM 87117; March, 1981.

2. Harrington, R. F., Time-Harmonic Electromagnetic Fields, McGraw-Hill Book Company, New York; 1961.

3. Harrington, R. F., Field Computations by Moment Methods, Macmillan, New York; 1968.

4. Butler, C. M., "Evaluation of potential integral at singularity of exact kernel in thin-wire calculations," IEEE Trans. on Antennas and Propagat., Vol. AP-23, No. 2, pp. 293-295; March, 1975.

5. Butler, C. M., and D. R. Wilton, "Analysis of various numerical techniques applied to thin-wire scatterers," IEEE Trans. on Antennas and Propagat., Vol. AP-23, No. 4, pp. 534-540; July, 1975.

6. Butler, C. M., D. R. Wilton, and A. W. Glisson, "Fundamentals of numerical solution methods in electromagnetics—short course notes," University of Mississippi, University, MS 38677; March, 1982.

7. Butler, C. M., and L. L. Tsai, "An alternate frill field formulation," IEEE Trans. on Antennas and Propagat., Vol. AP-21, No. 1, pp. 115-116; January, 1973.

8. Dwight, H. B., Tables of Integrals and Other Mathematical Data, Macmillan, New York; 1961.

9. Knopp, K., Theory and Application of Infinite Series (trans.), Hofner, New York; 1971.

10. Jolley, L. B. W., Summation of Series, Dover, New York; 1961.

11. Mack, R. B., "A study of circular arrays—radiation patterns and current distributions," Technical Report No. 383 (Vol. 3) ONR Contract Nonr-1866 (32)), Cruft Laboratory, Harvard University, Cambridge, MA, 1963.

12. C. M. Butler and C. A. Harrison, "An experimental study of cylindrical antennas radiating in or near a lossy half space," University of Mississippi, University, MS, Final Report—Volume 1 (Contract N66001-82-C-0045) to Naval Ocean Systems Center, San Diego, CA, June, 1983.


FILME
4-84